Atmos. Chem. Phys. Discuss., 15, 33407–33443, 2015
www.atmos-chem-phys-discuss.net/15/33407/2015/
doi:10.5194/acpd-15-33407-2015

Atmospheric Chemistry and Physics Discussions

Characteristics of aerosol pollution during heavy haze events in Suzhou, China

M. Tian[1], H. B. Wang[1], Y. Chen[1], F. M. Yang[1], X. H. Zhang[2], Q. Zou[2], R. Q. Zhang[2], Y. L. Ma[3], and K. B. He[3]

[1]Key Laboratory of Reservoir Aquatic Environment of CAS, Chongqing Institute of Green and Intelligent Technology, Chinese Academy of Sciences, Chongqing 400714, China
[2]Suzhou Environmental Monitoring Center, Suzhou 215004, China
[3]School of Environment, Tsinghua University, Beijing 100012, China

Received: 30 September 2015 – Accepted: 10 November 2015 – Published: 26 November 2015

Correspondence to: F. M. Yang (fmyang@cigit.ac.cn)

Published by Copernicus Publications on behalf of the European Geosciences Union.

Abstract

A comprehensive measurement was carried out to analyze the heavy haze events in Suzhou in January 2013 when extremely severe haze pollution occurred in many cities in China especially in the East. Hourly concentrations of $PM_{2.5}$, chemical composition (including water-soluble inorganic ions, OC, and EC), and gas-phase precursors were obtained via on-line monitoring system. Based on these data, detailed aerosol composition, light extinction and gas-phase precursors were analyzed to understand the characteristics of the haze events, moreover, the formation mechanism of nitrate and sulfate in $PM_{2.5}$ and the regional sources deduced from trajectory and PSCF were discussed to explore the origin of the heavy aerosol pollution. The results showed that frequent haze events were occurred on January 2013 and the concentrations of $PM_{2.5}$ often exceeded 150 $\mu g\,m^{-3}$ during the haze occurrence, with a maximum concentration of 324 $\mu g\,m^{-3}$ on 14 January 2013. Unfavorable weather conditions (high RH, and low rainfall, wind speed and atmospheric pressure), high concentration of secondary aerosol species (including SO_4^{2-}, NO_3^-, NH_4^+, and SOC) and precursors were observed during the haze events. Additionally, OM, $(NH_4)_2SO_4$, NH_4NO_3 were demonstrated to be the major contributors to the visibility impairment but the share differed from haze events. This study also found that the high concentration of sulfate might be explained by the heterogeneous reactions in the aqueous surface layer of pre-existing particles or in cloud processes while nitrate might be mainly formed through homogeneous gas-phase reactions. The results of trajectory clustering and the PSCF method manifested that aerosol pollutions in the studied areas were mainly affected by local activities and surrounding sources transported from nearby cities.

ACPD
15, 33407–33443, 2015

1 Introduction

High occurrence of haze events (visibility lower than 10 km under the conditions of relative humidity < 80 %) is of great concern to both scientists and public in China in recent years because of its great adverse effects on the people's health, traffic, climate, and other important aspects (Zhang et al., 2015; Charlson et al., 1987; Ramanathan and Vogelmann, 1997; Tegen et al., 2000; Yu et al., 2002; Tie et al., 2009a, b). Fine particle ($PM_{2.5}$, aerosols with an aerodynamic diameter of 2.5 microns or less) has a large impact on visibility by light extinction including scattering and absorbing solar and infrared radiation and is mainly responsible for the formation of haze(Yu et al., 2014). The light extinction of $PM_{2.5}$ is highly associated with the chemical compositions (Tao et al., 2014). Water-soluble inorganic ions and carbonaceous species often account for major fractions of $PM_{2.5}$ and are important contributors to visibility impairment (Tan et al., 2009; Pathak et al., 2009). Therefore, these species were emphatically investigated in researches related to haze occurrence (Yang et al., 2005; Jansen et al., 2014; Pathak et al., 2009). However, most of these studies were based on artificial sampling and off-line analysis which has its limits of providing detailed insight into the role of these species played during shorter haze periods.

High contributions of secondary inorganic aerosols (SIA, including sulfate, nitrate and ammonium), the predominant water-soluble ionic species in $PM_{2.5}$, to visibility reduction have been observed in many cities in China (Huang et al., 2014). Gas-phase or liquid-phase reaction of sulfur dioxide and nitrogen oxides is the primary source of aerosol sulfate and nitrate. For the formation of sulfate, homogeneous gas phase reaction of SO_2 with OH radical, heterogeneous reactions in the aqueous surface layer of pre-existing particles, and in-cloud processes are the primary mechanisms (Wang et al., 2006). The rates of gas-phase and liquid-phase reactions of SO_2 were close in summer while the heterogeneous processes were responsible for the oxidation in winter (Hewitt, 2001). Nitric acid can be formed from homogeneous gas-phase reactions of NO_2 with OH or O_3 and from heterogeneous hydrolysis of N_2O_5, which occurred

ACPD
15, 33407–33443, 2015

predominantly during daytime and nighttime respectively (Khoder, 2002). Both sulfuric acid and nitric acid will react with alkaline substance in the atmosphere, mostly ammonia under ambient conditions to produce salt (Hewitt, 2001). The neutralization of sulfuric acid by ammonia has been found to be preferred over the formation of ammonium nitrate (Warneck, 1999). Thus, the formation of ammonium nitrate in fine particles is usually under significantly neutralized or ammonium-rich sulfate conditions (Pathak et al., 2009). There are various factors influence the formation of aerosol sulfate and nitrate such as the levels of precursors (SO_2, NH_3, NO_x) and oxidants, the characteristics of pre-existing aerosols, and meteorological conditions. These factors may vary by location, this may result in different formation mechanism in different areas.

Due to the rapid economic and industrial developments and urbanization in past few decades, the visibility reduction become increasingly serious in China, especially in the East (Zhang et al., 2012). In January 2013, extremely severe, persistent and widespread haze occurred in 10 provinces, regions and cities in central and eastern China. These serious pollutions not only have great adverse effect on human health, caused a sharp increase in respiratory diseases, but also cause immeasurable economic loss (Huang et al., 2014; Chen et al., 2013). High secondary inorganic and organic aerosol contributions to particulate pollution during these haze events were reported in recent study based on the measurements at urban sites in Beijing, Shanghai, Guangzhou and Xi'an, which located in the northern, eastern, southern and western regions of China, respectively (Huang et al., 2014). This result indicated that in addition to investigate the primary particulate emissions, it's also important to explore the formation mechanism and effect factors of these secondary species in order to control $PM_{2.5}$ levels in China.

The Yangtze River Delta (YRD), together with the Pearl River Delta, Beijing–Tianjin–Tangshan and Sichuan Basin are of most interest as they are the four heaviest haze regions in China. The characteristics and formation mechanisms of haze in the Yangtze River Delta are different from other haze regions, such as Beijing and the Pearl River Delta (Fu et al., 2008). Suzhou located in the heartland of YRD region is an impor-

ACPD
15, 33407–33443, 2015

tant city in the YRD. Suzhou suffered the extremely serious aerosol pollution in January 2013. With the tremendous economic growth over the past 30 years, Suzhou experiences high levels of air pollution as reflected in the frequency of haze occurrence. The annually haze days in Suzhou increased from only two days to more than 150 days from 1956 to 2011, i.e. over 40 % of days are hazy in 2011. The lower visibility, particularly the haze, has become a major concern of the city, however, only few researches have been carried out to study the haze events in Suzhou. Little is known about the chemical characteristics and sources of fine particles in Suzhou. Therefore, an intensified monitoring campaign was launched from December 2012 to January 2013 to get insight into the haze occurrence in urban Suzhou. On the basis of high temporal resolution measurements combined with meteorological data, the objectives of this study are to (1) identify the dominant species in $PM_{2.5}$ and responsible for the visibility reduction, (2) explore the formation mechanism of the aerosol pollution, (3) study the impact of local and transport sources on the formation of haze in urban Suzhou.

2 Methodology

2.1 Field observations

The sampling station was set up at the roof of the building in Suzhou Institute of Environmental Sciences (31°20′ N, 120°36′ E) (Fig. 1), about 300 m west to Nanyuan South Road and 360 m north to S Ring Road Elevated Bridge. There is no industrial source nearby and this site is representative of an urban residential and commercial area. Suzhou is located in the center of Yangtze River Delta (YRD) and about 80 km east to Shanghai and 200 km west to Nanjing.

On-line hourly $PM_{2.5}$ mass concentrations, ionic species and OC/EC were measured by tapered element oscillating microbalance (TOEM), URG 9000 Ion Chromatography, Sunset semi-continuous OC/EC analyzer, respectively. Visibility was monitored by the Belfort Model 6000 Visibility Sensor.

ACPD
15, 33407–33443, 2015

2.2 Data analysis methods

2.2.1 Reconstruction of the light extinction coefficient

The light extinction (b_{ext}) which is the sum of light scattering by particle ($b_{s,p}$), absorption by particle ($b_{a,p}$), scattering by gas ($b_{s,g}$), and absorption by gas ($b_{a,g}$), is reconstructed according to the revised IMPROVE algorithm as following (Pitchford et al., 2007):

$$
\begin{aligned}
b_{ext} &= b_{s,p} + b_{a,p} + b_{a,g} + b_{s,g} \\
&\approx 2.2 \times f_S(RH) \times [\text{Small}\,(NH_4)_2SO_4] + 4.8 \times f_L(RH) \times [\text{Large}\,(NH_4)_2SO_4] \\
&+ 2.4 \times f_S(RH) \times [\text{Small}\,NH_4NO_3] + 5.1 \times f_L(RH) \times [\text{Large}\,NH_4NO_3] \\
&+ 2.8 \times [\text{Small OM}] + 6.1 \times [\text{Large OM}] \\
&+ 1 \times [\text{Fine Soil}] + 1.7 \times f_{SS}(RH) \times [\text{Sea Salt}] \\
&+ 0.6 \times [\text{Coarse Mass}] + 10 \times [\text{EC Mass}] \\
&+ 0.33 \times [NO_2(\text{ppb})] + \text{Rayleigh Scattering}
\end{aligned}
\tag{1}
$$

where f_S (RH) and f_L (RH) are the water growth factors for small- and large-sized distribution of sulfate and nitrate, respectively; f_{SS} (RH) is the water growth factor for sea salt. Water growth factors are adopted according to Pitchford et al. (2007). $(NH_4)_2SO_4$ mass is estimated by the SO_4^{2-} mass multiplied by a factor of 1.38, and the NH_4NO_3 mass is estimated by the NO_3^- mass multiplied by a factor of 1.29 based on the assumption that SO_4^{2-} and NO_3^- are fully neutralized by NH_4^+ in the forms of $(NH_4)_2SO_4$ and NH_4NO_3, respectively, according to the revised IMPROVE method. Organic matter (OM) is derived from multiplying OC concentrations by a factor of 1.8 to account for unmeasured atoms.

The concentrations of sulfate, nitrate, and OM are divided into small- and large-sized fractions in this algorithm. The size modes are described by log-normal mass size distributions with geometric mean diameter and geometric standard deviations.

ACPD
15, 33407–33443, 2015

Concentrations of sulfate, nitrate, and OM in the large- and small-mode are estimated by using the following equations (taking sulfate as an example):

$$[\text{Large}\,(NH_4)_2SO_4] = [\text{Total}\,(NH_4)_2SO_4]^2/20, \text{ for } [\text{Total}\,(NH_4)_2SO_4] < 20\,\mu g\,m^{-3} \quad (2)$$

$$[\text{Large}\,(NH_4)_2SO_4] = [\text{Total}\,(NH_4)_2SO_4], \text{ for } [\text{Total}\,(NH_4)_2SO_4] > 20\,\mu g\,m^{-3} \quad (3)$$

$$[\text{Small}\,(NH_4)_2SO_4] = [\text{Total}\,(NH_4)_2SO_4] - [\text{Large}\,(NH_4)_2SO_4] \quad (4)$$

2.2.2 Air mass back trajectory

To study the impact of local and regional sources on the aerosol pollution in Suzhou, the 48 h back trajectories starting at 100 m from the sampling site were calculated by using the NOAA HYSPLIT model (http://ready.arl.noaa.gov/HYSPLIT_traj.php). The back trajectories were calculated four times per day at starting times of 04:00, 10:00, 16:00, and 22:00 UTC, i.e. 12:00, 18:00, 00:00, and 06:00 LT, respectively. The trajectory cluster analysis was based on the GIS-based software TrajStat (Wang et al., 2009).

2.2.3 Potential source contribution function

The potential source contribution function (PSCF) method is based on the results of HYSPLIT model and can be used to identify the regional sources. The zone of concern is divided into $i \times j$ small equal grid cells. The PSCF value for the ijth grid cell is calculated as: $PSCF_{ij} = m_{ij}/n_{ij}$, where n_{ij} is designated as the number of trajectory segment endpoints that fall in the ijth cell and m_{ij} is defined as the number of trajectory endpoints with pollutants concentrations higher than an set criterion (Ashbaugh et al., 1985; Wang et al., 2009). In present study, the average concentrations were treated as the criterion (Hsu et al., 2003). The PSCF values were multiplied by a weighting function W_{ij} to reduce the effect of small values of n_{ij} and to better reflect the uncertainty in the values for the cells with small n_{ij} values. The weighting function W_{ij} is defined

ACPD
15, 33407–33443, 2015

as follows (Polissar et al., 1999):

$$W_{ij} = \begin{cases} 1.00, 80 < n_{ij} \\ 0.70, 20 < n_{ij} \leq 80 \\ 0.42, 10 < n_{ij} \leq 20 \\ 0.05, n_{ij} \leq 10 \end{cases}$$

The PSCF value can be interpreted as the conditional probability that the air masses with pollutants concentration greater than the set criterion pass through the *ij*th cell during transport to the receptor site (Wang et al., 2009). That is, cells with high PSCF values are indicative of regions have high potential contributions to the pollution at the receptor site.

3 Results and discussion

3.1 General characteristics of haze events

As illustrated in Fig. 2, the visibility varied from a few hundred meters to more than 50 km with a minimum value of only 322 m on 15 January 2013, which was accompanied by high RH (82 %). During the 2-month observation period, there were totally ten periods when visibility below 10 km. Except for the five periods which were accompanied by precipitation, five haze events were identified and all occurred in January 2013. During the haze occurrence, the hourly concentrations of $PM_{2.5}$ often exceeded 150 $\mu g\,m^{-3}$, with a maximum concentration of 324 $\mu g\,m^{-3}$ on 14 January 2013, were generally higher than normal periods. The daily concentrations of $PM_{2.5}$ on haze days varied from 148 to 196 $\mu g\,m^{-3}$, which were 1.97 to 2.61 times the Grade II criteria of the national ambient air quality standard (75 $\mu g\,m^{-3}$). This was comparable to the $PM_{2.5}$ concentrations in Nanjing with average value of 175.6 $\mu g\,m^{-3}$ but little higher than some other cities in YRD with the mean values lower than 147.3 $\mu g\,m^{-3}$ when haze

ACPD
15, 33407–33443, 2015

occurred in January 2013 (H. Wang et al., 2014a, Y. Wang et al., 2014). The aerosol pollution happened in northeast China such as Beijing, Tianjin, and Shijiazhuang were much severer, for instance, the daily and hourly concentrations of $PM_{2.5}$ were up to 368 and 462 $\mu g\,m^{-3}$ in Tianjin in 9 to 13 January 2013; the hourly maximum values of approximately 1000 $\mu g\,m^{-3}$ were recorded in Beijing and Shijiazhuang in January 2013 (Ji et al., 2014; Han et al., 2014; Wang et al., 2015).

The duration of haze events comprised approximately 40 % of whole January 2013, whereas no haze appeared in December 2012. Less rainfall in the January might be one of the causes. The relative humidity (RH) was reported to be an important contributor to the visibility reduction. In present study, the RH increased with the reduction of visibility, e.g. when RH increased from 42 to 78 %, the visibility decreased from 42 km at 2:00 p.m. on 17 January to 4 km at 7:00 a.m. on 19 January. Statistically, the RH was relatively higher during haze occurrence than clear periods. Low wind speeds, smaller than 5 $m\,s^{-1}$, were frequently observed during this winter. Furthermore, the wind speeds were mostly less than 1 $m\,s^{-1}$ during the haze events, lower than those in Beijing (Yang et al., 2015). Besides, atmospheric pressure was also found to be relatively low during the haze occurrences. The stagnant air, low wind speed and pressure, was unfavorable for the horizontal transport or vertical diffusion of aerosols, and therefore leading to the increase of aerosol concentration. Therefore, unfavorable weather conditions (high RH, and low rainfall, wind speed and atmospheric pressure) might provide external cause beneficial for the formation of haze in January 2013 in Suzhou as in many other cities (H. Wang et al., 2014b; J. Wang et al., 2014; Y. Wang et al., 2014; Han et al., 2014; Yang et al., 2015).

In order to get more insights of the haze formation in this region, three haze events, which occurred on 19 January, from 21 to 26 January, and on 30 January, respectively, were further discussed below.

ACPD
15, 33407–33443, 2015

3.2 $PM_{2.5}$ chemical composition and light extinction

3.2.1 $PM_{2.5}$ chemical composition

The temporal variations of the concentrations of water-soluble inorganic ions (WSIIs) were illustrated in Fig. 3. The mean concentration of WSIIs (including four anions and five cations) was $48.8 \pm 24.6\,\mu g\,m^{-3}$, accounting for 40 % of $PM_{2.5}$ mass concentration, little lower than that in Beijing which was $69.4 \pm 55.8\,\mu g\,m^{-3}$ and accounted for 43 % of $PM_{2.5}$ (Tao et al., 2015). SO_4^{2-} was the most abundant species in WSIIs, with averaged value of $21.1 \pm 13.5\,\mu g\,m^{-3}$, followed by NH_4^+ ($13.9 \pm 5.69\,\mu g\,m^{-3}$) and NO_3^- ($10.7 \pm 6.75\,\mu g\,m^{-3}$), accounting for 43, 29 and 21 % of WSIIs, respectively. These secondary inorganic components totally constitute 93 % of total WSIIs close to the result in Beijing (Gao et al., 2015; Tao et al., 2015). The rest of ions, Na^+ ($1.36 \pm 0.43\,\mu g\,m^{-3}$), K^+ ($0.85 \pm 0.45\,\mu g\,m^{-3}$), Cl^- ($0.54 \pm 1.28\,\mu g\,m^{-3}$), Ca^{2+} ($0.34 \pm 0.27\,\mu g\,m^{-3}$), F^- ($0.06 \pm 0.72\,\mu g\,m^{-3}$), Mg^{2+} ($0.05 \pm 0.07\,\mu g\,m^{-3}$), each had minor contribution (< 3 %) to WSIIs.

NO_3^- and SO_4^{2-} are mainly formed from the transformation of their precursors of NO_x and SO_2 (Wang et al., 2005). The emission ratio of NO_x to SO_2 was 17.2–52.6 for motor vehicles and 0.527–0.804 for stationary sources in the Yangtze River Delta, which means that the emissions of SO_2 from motor vehicles were much less than NO_x, but the emissions of SO_2 from stationary sources such as power plants, industrial boilers and furnaces were relatively higher than NO_x (Fu et al., 2008). Thus, the mass ratio of NO_3^-/SO_4^{2-} could be used as an indicator of the relative importance of mobile and stationary sources of sulfur and nitrogen in the atmosphere (Arimoto et al., 1996). In present study, the averaged ratios of NO_3^-/SO_4^{2-} and NO_x/SO_2 were 0.59 and 5.68, respectively, indicating that emissions from vehicles and stationary sources were both important in Suzhou. The ratios of NO_3^-/SO_4^{2-} in this study were lower than the ratio in Beijing but higher than those reported in Shanghai (0.43), Qingdao (0.35), Taiwan (0.20), and Guiyang (0.13) (Wang et al., 2006; Yao et al., 2002; Hu et al., 2002a; Fang et al., 2002; Xiao and Liu, 2004).

ACPD
15, 33407–33443, 2015

The NO_3^-/SO_4^{2-} ratio was relatively higher for 20 % worst visibility than 20 % best visibility, which were 0.58 and 0.54, respectively, suggesting that vehicle emission might play an important role in haze pollution. This was in agreement with the result in Guangzhou, where the NO_3^-/SO_4^{2-} ratio was 1.02 under stagnation and 0.55 in normal days, but contrary to that in Beijing, where the ratio in haze days (0.64) was lower than in normal days (0.83) (Tan et al., 2009; Wang et al., 2006). Besides of lower NO_3^-/SO_4^{2-} ratio, Wang et al. also found lower NO_2/SO_2 ratio and lower ratio of (NO_3^-/SO_4^{2-}) to (NO_2/SO_2) in haze days than that in clear days in Beijing, and summarized that the formation rate of nitrate might not be the controlling factor for the nitrate concentrations in $PM_{2.5}$ (Wang et al., 2006). The low NO_3^-/SO_4^{2-} ratios found in haze days in Beijing was considered to be related to the thermodynamic characteristic of NH_4NO_3 (Wang et al., 2006). The ratios of NO_x/SO_2 in present study were 6.89 for 20 % worst visibility period higher than 4.30 for 20 % best visibility period. The ratios of (NO_3^-/SO_4^{2-}) to (NO_x/SO_2) were also lower for worse visibility period in present study, suggesting that the nitrate concentrations may be also greatly affected by the re-volatilization of NH_4NO_3 as those in Beijing.

The carbonaceous species, constituting 22 % of $PM_{2.5}$, were dominated by organic carbons, which were $22.8 \pm 10.6\,\mu g\,m^{-3}$ and 3 to 29 times that of elemental carbon ($2.79 \pm 2.58\,\mu g\,m^{-3}$), similar to those in Beijing (Tao et al., 2015). The relatively high ratios of OC/EC (10.6 ± 4.29) which were higher than the ratios in Beijing (7.1 ± 0.5) and Jinan (7.15 ± 1.78) demonstrated the existence of secondary organic carbon (SOC) (Ji et al., 2014; Zhang et al., 2014). The concentrations of SOC were estimated by applying the EC tracer method, which has been widely used to estimate the secondary organic aerosol contribution to $PM_{2.5}$ concentrations (Castro et al., 1999; Yang et al., 2005). The minimum ratio of OC/EC was 3.09 in present study. So the estimated concentrations of SOC were $14.2 \pm 5.69\,\mu g\,m^{-3}$, contributing 65 % on average to OC. The ratios of SOC/OC were higher than 0.5 during almost the whole sampling time except for the periods around 30 January, when the third haze event occurred. This

ACPD
15, 33407–33443, 2015

ratio was higher than most of the results found in other areas such as Beijing and Guangzhou (Yang et al., 2005; Tan et al., 2009).

Overall, according to the percentage of each species in $PM_{2.5}$ mass, the major components in $PM_{2.5}$ were SO_4^{2-} (17 %), SOC (14 %), NH_4^+ (12 %), NO_3^- (8 %), and POC (6 %) with total percentage of 57 %. It is noted that the first four species were mainly from secondary sources. In addition, the concentrations of $PM_{2.5}$ were significantly correlated with these secondary species, revealing that gas to particle conversion during winter in this region was severe and had great impact on aerosol pollution in this region.

3.2.2 Variations of aerosol particles and precursors

Figure 4 diagrammed the diurnal variation of meteorological parameters, various aerosol components and the precursors under three different visibility conditions (i.e., (1) all data, (2) visibility ≤ 10 km, (3) visibility > 10 km). The daily variation of gas-phase compounds were different between species and were mainly controlled by the direct surface emissions (such as NO_x, SO_2, and CO) or photochemical process (O_3). There were a distinct AM peak and a less distinct PM peak, consistent with morning and PM rush hour for NO_x and CO. This might related to the heavy traffic emission in the rush hours and the strong elevation of the Planetary Boundary Layer heights at noon. In contrast, there was only one mid-day peak for SO_2. This diurnal profiles were similar to those observed in Guangzhou (Hu et al., 2002b) and Maryland (Antony Chen et al., 2001). In the latter study, the dominant source of SO_2 was considered to be the long range transport from the industrialized Midwest and with the deep boundary layer around noon, SO_2 aloft mixed more effectively down to the surface and thus caused the mid-day peak of SO_2. The reasons for the diurnal variation of SO_2 observed in present study need further investigation. Similar to the diurnal distribution of SO_2, O_3 also showed one distinct peak around noon due to the strong photochemistry at that time (Quan et al., 2014).

For the aerosol components, EC which was also produced by the surface emissions showed similar profile to NO_x and CO. Furthermore, EC had significantly positive cor-

ACPD
15, 33407–33443, 2015

relation with NO_x and CO, demonstrating that they had common sources, mainly from vehicular exhaust. However, the diurnal profiles of the secondary species were similar to their precursors but obviously affected by O_3 concentrations, as these species were mainly produced by chemical processes. For instance, there was a 2 h delay for sulfate to reach its peak compared to SO_2 due to the transformation. This pattern was also observed in Guangzhou (Hu et al., 2002b). NO_3^- and SOC exhibited similar diurnal variation as their precursors had common sources and they both formed from secondary photochemical oxidation. The daily profiles of NO_3^-, NH_4^+ and SOC showed lower concentrations around 15:00 LT probably due to the high boundary layer and/or low concentration of precursors. Besides, for NO_3^- and NH_4^+, high temperature, which enhanced the evaporative loss, and low relative humidity may also responsible for the low level.

Figure 4 also suggested that both gas-phase compounds and aerosol components all showed similar pattern of diurnal variation but had different magnitudes of concentrations for different visibility levels. These components except for O_3 all showed relatively higher concentrations under low visibility especially for the secondary inorganic species, indicating the important impact of the formation of secondary components on the visibility reduction. The relatively low levels of O_3 under low visible conditions might because of the decreased photochemical production and the chemical conversions of SO_2 and NO_x to sulfate and nitrate. It is worth noting that relatively high humidity which favored for the formation of sulfate and nitrate was observed under low visibility conditions. In addition, it seemed that low visibility was associated with southwest wind.

3.2.3 Light extinction coefficient

In order to appoint the contribution of $PM_{2.5}$ constituents to the visibility degradation, light extinction (b_{ext}) was reconstructed based on the revised IMPROVE algorithm. In the present study, the impact of fine soil and coarse mass were not included because the lack of metal element and coarse matter concentrations. Thus, the revised

ACPD
15, 33407–33443, 2015

IMPROVE algorithm was modified as following:

$$
\begin{aligned}
b_{\mathrm{ext}} &= b_{\mathrm{s,\,p}} + b_{\mathrm{a,\,p}} + b_{\mathrm{a,\,g}} + b_{\mathrm{s,\,g}} \\
&\approx 2.2 \times f_{\mathrm{S}}(\mathrm{RH}) \times [\mathrm{Small}\,(\mathrm{NH_4})_2\mathrm{SO_4}] + 4.8 \times f_{\mathrm{L}}(\mathrm{RH}) \times [\mathrm{Large}\,(\mathrm{NH_4})_2\mathrm{SO_4}] \\
&+ 2.4 \times f_{\mathrm{S}}(\mathrm{RH}) \times [\mathrm{Small}\,\mathrm{NH_4NO_3}] + 5.1 \times f_{\mathrm{L}}(\mathrm{RH}) \times [\mathrm{Large}\,\mathrm{NH_4NO_3}] \\
&+ 2.8 \times [\mathrm{Small\ OM}] + 6.1 \times [\mathrm{Large\ OM}] \\
&+ 1.7 \times f_{\mathrm{SS}}(\mathrm{RH}) \times [\mathrm{Sea\ Salt}] + 10 \times [\mathrm{EC\ Mass}] + 0.33 \times [\mathrm{NO_2(ppb)}] + \mathrm{Rayleigh\ Scattering}
\end{aligned}
$$

The estimated b_{ext} in present study were $664 \pm 288\,\mathrm{M\,m^{-1}}$, significantly correlated with $PM_{2.5}$ concentrations ($r = 0.94$, $p < 0.001$). Visibility is inversely correlated with the extinction coefficient according to the Koschmieder equation (Vis $= K/b_{\mathrm{ext}}$). By using a K value of 3.912, we further calculated the visibility based on the reconstructed b_{ext}. The estimated visibilities were 7.47 ± 4.12 km, ranged from 2.57 to 23.41 km. Although this was lower than the measured visibility, which were 15.0 ± 8.50 km, the estimated and measured visibility had similar temporary trend and were significantly correlated with each other ($r = 0.71$, $p < 0.001$).

The light extinction were mostly influenced by aerosol light scattering as the estimated $b_{\mathrm{s,\,p}}$ were $609 \pm 277\,\mathrm{M\,m^{-1}}$, accounting for 91 % of the b_{ext} (at least 75 %), while $b_{\mathrm{a,\,p}}$ and the extinction coefficient by gaseous were only 27.9 ± 25.8 and $26.6 \pm 4.87\,\mathrm{M\,m^{-1}}$. The largest contributor of reconstructed chemical species in fine particles to b_{ext} was organic matter (OM), accounting for 40 %, followed by $(NH_4)_2SO_4$, NH_4NO_3, and EC with their shares of 34, 16 and 4 %, respectively. Fractions of these contributors varied greatly over the study period, e.g. the contributions of NH_4NO_3 ranged from only 3 % to up to 40 %. Generally, the contributions of $(NH_4)_2SO_4$ and NH_4NO_3 were higher under low visibility period, increased from 30 and 11 % under 20 % best visibility period to 39 and 19 % under 20 % worst visibility period, increased 1.3 and 1.7 times, respectively. While the contributions of OM and EC were reduced from 46 and 5 % un-

ACPD
15, 33407–33443, 2015

der 20 % best visibility period to 35 and 4 % under 20 % worst visibility period. These results indicated the important role of sulfate and nitrate played on haze formation.

The percentages of the aerosol components contribute to the light extinction were also experienced different variations in their fractions during different haze events. We compared the contributions of these components under 20 % best visibility conditions to those under 20 % worst visibility conditions to investigate the controlling factor for the haze formation (Fig. 5). During the first haze event (on 19 January), the contributions of NH_4NO_3 increased from only 8 % under 20 % best visibility to 24 % under 20 % worst visibility while the percentage of OM decreased from 48 to 37 %. For $(NH_4)_2SO_4$ and EC, there was no significant change. For the second haze event (from 21 to 26 January), the fractions were 1.8, 1.5 and 1.3 times higher for NH_4NO_3, $(NH_4)_2SO_4$ and EC respectively but 1.2 times lower for OM under worse visibility condition. Overall, $(NH_4)_2SO_4$ made great contribution to the light extinction and NH_4NO_3 had largest difference between 20 % best and worst visibility conditions. Therefore, secondary inorganic aerosol especially NH_4NO_3 was likely the key component for the impaired visibility for these two haze events. The elevated proportion of $(NH_4)_2SO_4$ and NH_4NO_3 during the heavy polluted period was also observed in Beijing (Tao et al., 2015; Wang et al., 2015; Zheng et al., 2015). Contrarily, during the third haze (on 30 January) increasing proportions of OM and EC (from 40 to 49 % and 6.8 to 11 %, respectively) accompanied with decreasing percentage of $(NH_4)_2SO_4$ (from 28 to 19 %) were found under worse visibility period, indicating that the carbonaceous components might be relatively important for the visibility reduction. Therefore, there seems to be different formation mechanisms for haze formation in Suzhou.

3.3 Conversion from gas to particle phase

As discussed earlier, the chemical formation of sulfate and nitrate from SO_2 and NO_2 should play important role for visibility reduction. The sulfur oxidation ratio, defined as $SOR = n\text{-}SO_4^{2-}/(n\text{-}SO_4^{2-} + n\text{-}SO_2)$ and the nitrogen oxidation ratio, defined as $NOR = n\text{-}NO_3^-/(n\text{-}NO_3^- + n\text{-}NO_2)$ were used as indicators of the secondary transformation pro-

ACPD
15, 33407–33443, 2015

cesses. Both SOR and NOR were higher with lower visibility (Fig. 6), implying greater oxidation of gaseous species and more elevated secondary aerosols. This was supported by the higher concentrations of SO_4^{2-}, NH_4^+, and NO_3^- under worse visibility conditions. The daily variation of NOR showed similar pattern as NH_4^+ and NO_3^-, likewise, SOR had similar diurnal change as SO_4^{2-}, indicating the influence from NO_x or SO_2 and O_3. Additionally, it is interesting to notice that under low visibility conditions during nighttime when O_3 concentrations were extremely low, there was still a rapid chemical conversion from gaseous to particle phase especially for sulfate particles. This conversion might mainly be produced through the processes other than the photochemical activities such as heterogeneous reactions in the aqueous surface layer of pre-existing particles or in cloud processes. The higher humidity during that time and the significant positive correlations between SOR and humidity through the whole study period again seem to validate that the heterogeneous process likely dominate the sulfate formation. This was consistent with the finding by Hewitt that liquid phase chemical conversion process was responsible for the formation of sulfate particles in winter (Hewitt, 2001).

Compared to the formation of sulfate, the contributions of various conversion pathways to nitrate formation were less known (Pathak et al., 2009). In this section, we examined in detail the possible causes of nitrate in $PM_{2.5}$. Figure 7 showed the nitrate-to-sulfate molar ratio ($[NO_3^-]/[SO_4^{2-}]$) as a function of the ammonium-to-sulfate molar ratio ($[NH_4^+]/[SO_4^{2-}]$), which can provide an insight into the formation pathway of the secondary species (Jansen et al., 2014; Pathak et al., 2009).

The relative abundance of nitrate linearly increased with the increasing ammonium-to-sulfate molar ratio. Fitting a linear regression line resulted in an intercept of $[NH_4^+]/[SO_4^{2-}]$ axis of 1.51, indicating that nitrate formation via homogeneous reaction of HNO_3 with NH_3 became significant at $[NH_4^+]/[SO_4^{2-}] > 1.51$ (Pathak et al., 2004; Pathak and Chan, 2005). Pathak et al. (2009) also reported an intercept value of 1.5 for a variety of cities worldwide while Jansen et al. (2014) found a little smaller intercept value of 1.38 for Hangzhou. The ammonium concentration in excess of the amount at

ACPD
15, 33407–33443, 2015

which nitrate formation became evident was defined as excess ammonium ($[NH_4^+]_{exc}$ = $([NH_4^+]/[SO_4^{2-}]-1.51)\times[SO_4^{2-}]$). The concentrations of excess ammonium were always higher than 0 and linearly correlated with nitrate concentration, as shown in Fig. 8. This indicated that the formation of nitrate was strongly associated with ammonium formation. In other words, when the excess ammonium was > 0, the gas-phase homogeneous reaction between the ambient ammonia and nitric acid was responsible for forming nitrate (Pathak et al., 2009; Jansen et al., 2014). The slope of 0.37 for the regression and the scattering of the data indicated that the excess ammonium was bound to species other than nitrate, such as chloride, bisulfate etc. The significance of gas-phase homogeneous reaction to nitrate formation has been reported for many cities (Jansen et al., 2014; Pathak et al., 2009). Besides, a model study also verified that aqueous-phase oxidation of NO_x was of minor importance for nitrate production in the atmosphere (Pandis and Seinfeld, 1989). But contrarily, heterogeneous reactions were considered to be significantly important in the production of both sulfate and nitrate (Zheng et al., 2015).

3.4 Regional sources deduced from trajectory and PSCF analyses

The regional sources and transport of air pollutants exert a profound impact on local air quality in YRD region as it is located in the typical monsoon region (Ding et al., 2013). Therefore, trajectory clustering method was employed to examine the pathway of air mass and to look into the difference of chemical compositions and light extinction coefficients among the air mass with different origination. The calculated 48 h back trajectories were clustered into six clusters (Fig. 9), i.e. six air mass transport pathways. Table 1 summarized the percentage of trajectories for each trajectory cluster and the corresponding mean concentrations of $PM_{2.5}$ and major aerosol species. The trajectory clusters were dominated by cluster 2, accounting for 31.7 %, followed by cluster 1 and 3, both accounted for 20.6 %, and the rest clusters, cluster 4, 5 and 6 accounted for

ACPD
15, 33407–33443, 2015

12.7, 6.3 and 7.9 %, respectively. Obviously, air masses mainly originated from the north and southwest (cluster 1 to 4).

The mean concentrations of $PM_{2.5}$ and main aerosol species varied with certain types of air masses. The highest mean concentration of $PM_{2.5}$ (167 $\mu g\,m^{-3}$) was associated with C3 cluster with the air masses originating from northwest and passed over Anhui and Jiangsu provinces. The air from the C1, C2 and C4 areas were also related to relatively high $PM_{2.5}$ concentrations, which were 129, 117 and 103 $\mu g\,m^{-3}$ respectively. These air masses all passed over some highly industrialized cities, such as Qingdao, Nanjing, and Hangzhou (Fig. 1). Relatively low concentrations of $PM_{2.5}$ were associated with clusters C5 (84 $\mu g\,m^{-3}$) and C6 (87 $\mu g\,m^{-3}$). The trajectories of C5 and C6 mostly originated from southeast and northeast respectively. Based on the pathways and origins, these air masses were expected to bring in relatively clean air from the East China Sea and the Yellow Sea and consequently reduce the aerosol pollution in Suzhou.

For the major components in $PM_{2.5}$, the highest averaged concentrations were associated with C3 cluster for sulfate, nitrate and ammonium but with C5 cluster for both OC and EC. Accordingly, the composition profiles of these major species were different between clusters. C1, C2, C3 and C4 trajectory clusters had similar composition with relatively higher fractions of secondary inorganic ions (secondary inorganic ions > 35 %, OC < 19 %) compared to C5 and C6 clusters which both had relatively high contribution of OC (secondary inorganic ions < 30 %, OC > 23 %). These differences of $PM_{2.5}$ concentrations and compositions in different clusters may result in distinct light extinction coefficients and species contributions to visibility reduction when air mass originated from different directions (Fig. 9). Similar to $PM_{2.5}$, b_{ext} values were higher when the air masses originated from the Northwest area (C3), whereas b_{ext} were relatively low when air masses fell into C5 and C6 areas. AS and OM were the dominated species determining the light extinction for all clusters. However, differently, AS was the predominant contributor to light extinction for trajectories from north and northwest (C1, C3, C4), while in other cases the light extinction was primarily affected

ACPD
15, 33407–33443, 2015

by OM. AN was the third highest contributor in all trajectory clusters with the largest contribution when air mass originated from northwest.

The origins of air mass in different haze events were further analyzed to interpret the relative contribution of chemical species to visibility reduction differed in haze events. Most air mass fell into C1 and C3 (air mass from north and northwest) in the first two haze occurrence while all air mass trajectories were in C2 (air mass from south) for the third haze event. The contribution of OM to the total light extinction was higher in the third haze event than the first two as discussed early, consistent with the results for cluster analysis that the light extinction was primarily impacted by AS for C1 and C3 but by OM for C2. These results manifested that the air mass originated from southwest and passed over Zhejiang province might play a key role in the high contribution of OM in the third haze event.

It should be noted that air mass back trajectory analysis only suggest the originations and pathways of air mass but not directly reveal the exact sources. Based on the results of trajectory analysis, the PSCF method was applied to explore the likely regional sources of major components in $PM_{2.5}$, including sulfate, nitrate, OC, and EC, as illustrated in Fig. 10. Generally, $PM_{2.5}$ and the five aerosol species in Suzhou were mainly affected by local sources and nearby cities. Specifically, the higher value for $PM_{2.5}$ and the aerosol components were all localized in northwest to the south, covering surrounding cities in Jiangsu and near the border of Anhui and Zhejiang provinces. Additionally, these species were all affected by pollutions from Anhui province. Sulfate, nitrate and ammonium had similar spatial distribution, and relatively more affected by the north and northwest cities in Shandong, Jiangsu and Anhui provinces while pollutions from south cities in Zhejiang province had more impact on OC and EC in studied area than sulfate, nitrate and ammonium.

ACPD
15, 33407–33443, 2015

4 Conclusions

Heavy aerosol pollution occurred in Suzhou in January 2013 with daily $PM_{2.5}$ concentrations on haze days 1.97 to 2.61 times higher than Grade II criteria of the national ambient air quality standard (75 $\mu g\,m^{-3}$) and maximum value of 324 $\mu g\,m^{-3}$ on 14 January 2013. Unfavorable weather conditions (high RH, low rainfall, wind speed and atmospheric pressure) especially high RH might provide beneficial conditions for these haze formation.

WSII and carbonaceous species both increased during the haze events and the major compositions were SO_4^{2-}, NO_3^-, NH_4^+, and SOC, which were mainly from secondary sources, revealing severe gas to particle conversion during winter in this region. The conversion mechanisms were further analyzed for sulfate and nitrate. Rapid chemical conversion from gas to particle phase for sulfate particles under extremely low O_3 concentrations and significant correlations between SOR and humidity demonstrated that heterogeneous process might dominate the sulfate formation. However, the result of ($[NO_3^-]/[SO_4^{2-}]$) as a function of ($[NH_4^+]/[SO_4^{2-}]$) showed that the formation of ammonium nitrate via the homogeneous gas-phase reaction was favored.

The reconstructed light extinction coefficients based on the revised IMPROVE algorithm were $664 \pm 288\,M\,m^{-1}$, and mainly contributed by OM (40 %), $(NH_4)_2SO_4$ (34 %), NH_4NO_3 (16 %), and EC (4 %). The contributions of these species experienced different variations in their fractions under different visibility conditions. Generally, the share of $(NH_4)_2SO_4$ and NH_4NO_3 were higher under low visibility conditions while the percentages of OM and EC were increased under high visibility conditions, indicating that secondary inorganic aerosols especially NH_4NO_3 seemed to be very important for the impaired visibility. But distinctively, increasing proportions of OM and EC accompanied with decreasing percentage of $(NH_4)_2SO_4$ were found under worse visibility when the third haze occurred, suggesting that the carbon components might be relatively important for the visibility reduction for this haze event. These differences in different haze

ACPD
15, 33407–33443, 2015

events might be greatly affected by the pathways of air masses according to trajectory clustering analysis.

The result of trajectory clustering analysis showed that the air quality in Suzhou was mostly affected by air masses originating from North and Southwestern areas which were associated with high aerosol concentrations. Distinct aerosol composition profiles, light extinction coefficients and species contributions to visibility reduction were observed when air mass originated from different directions, e.g. AS was the predominant contributor to light extinction for trajectories from north and northwest, while in other cases the light extinction was primarily affected by OM.

The likely sources of aerosol and the major species based on the PSCF method were mainly from local anthropogenic activities and source emissions transported from nearby cities. The northwestern to southern regions may be important sources of aerosols and the major components. The northern and northwestern areas were predominant source regions for sulfate, nitrate and ammonium aerosols, whereas the southern area could be the common source region for carbonaceous species. This information has the implications for the importance of collaborative air pollution control strategy in the Yangtze River Delta Region.

Acknowledgements. This work was supported by the National Natural Science Foundation of China projects (41403089, 41375123), the "Strategic Priority Research Program" of the Chinese Academy of Sciences (KJZD-EW-TZ-G06-04), and the State Environmental Protection Key Laboratory of Sources and Control of Air Pollution Complex (SCAPC201310).

References

Antony Chen, L. W., Doddridge, B. G., Dickerson, R. R., Chow, J. C., Mueller, P. K., Quinn, J., and Butler, W. A.: Seasonal variations in elemental carbon aerosol, carbon monoxide and sulfur dioxide: implications for sources, Geophys. Res. Lett., 28, 1711–1714, doi:10.1029/2000gl012354, 2001.

Arimoto, R., Duce, R. A., Savoie, D. L., Prospero, J. M., Talbot, R., Cullen, J. D., Tomza, U., Lewis, N. F., and Jay, B. J.: Relationships among aerosol constituents from

ACPD

15, 33407–33443, 2015

Asia and the North Pacific during PEM-West A, J. Geophys. Res.-Atmos., 101, 2011–2023, doi:10.1029/95jd01071, 1996.
Ashbaugh, L. L., Malm, W. C., and Sadeh, W. Z.: A residence time probability analysis of sulfur concentrations at Grand-Canyon-National-Park, Atmos. Environ., 19, 1263–1270, doi:10.1016/0004-6981(85)90256-2, 1985.
Castro, L. M., Pio, C. A., Harrison, R. M., and Smith, D. J. T.: Carbonaceous aerosol in urban and rural European atmospheres: estimation of secondary organic carbon concentrations, Atmos. Environ., 33, 2771–2781, doi:10.1016/S1352-2310(98)00331-8, 1999.
Charlson, R. J., Lovelock, J. E., Andreae, M. O., and Warren, S. G.: Oceanic phytoplankton, atmospheric sulfur, cloud albedo and climate, Nature, 326, 655–661, doi:10.1038/326655a0, 1987.
Chen, R., Zhao, Z., and Kan, H.: Heavy smog and hospital visits in Beijing, China, Am. J. Resp. Crit. Care, 188, 1170–1171, doi:10.1164/rccm.201304-0678LE, 2013.
Fang, G. C., Chang, C. N., Wu, Y. S., Fu, P. P. C., Yang, C. J., Chen, C. D., and Chang, S. C.: Ambient suspended particulate matters and related chemical species study in central Taiwan, Taichung during 1998–2001, Atmos. Environ., 36, 1921–1928, doi:10.1016/S1352-2310(02)00187-5, 2002.
Fu, C. B., Yang, X. Q., Sun, J. N., Zheng, L. F., Xie, Y. N., Herrmann, E., Nie, W., Petäjä, T., Kerminen, V.-M., and Kulmala, M.: Ozone and fine particle in the western Yangtze River Delta: an overview of 1 yr data at the SORPES station, Atmos. Chem. Phys., 13, 5813–5830, doi:10.5194/acp-13-5813-2013, 2013.
Fu, Q., Zhuang, G., Wang, J., Xu, C., Huang, K., Li, J., Hou, B., Lu, T., and Streets, D. G.: Mechanism of formation of the heaviest pollution episode ever recorded in the Yangtze River Delta, China, Atmos. Environ., 42, 2023–2036, doi:10.1016/j.atmosenv.2007.12.002, 2008.
Gao, J., Tian, H., Cheng, K., Lu, L., Zheng, M., Wang, S., Hao, J., Wang, K., Hua, S., Zhu, C., and Wang, Y.: The variation of chemical characteristics of $PM_{2.5}$ and PM_{10} and formation causes during two haze pollution events in urban Beijing, China, Atmos. Environ., 107, 1–8, doi:10.1016/j.atmosenv.2015.02.022, 2015.
Han, S., Wu, J., Zhang, Y., Cai, Z., Feng, Y., Yao, Q., Li, X., Liu, Y., and Zhang, M.: Characteristics and formation mechanism of a winter haze-fog episode in Tianjin, China, Atmos. Environ., 98, 323–330, doi:10.1016/j.atmosenv.2014.08.078, 2014.
Hewitt, C. N.: The atmospheric chemistry of sulphur and nitrogen in power station plumes, Atmos. Environ., 35, 1155–1170, doi:10.1016/S1352-2310(00)00463-5, 2001.

ACPD
15, 33407–33443, 2015

Hsu, Y. K., Holsen, T. M., and Hopke, P. K.: Comparison of hybrid receptor models to locate PCB sources in Chicago, Atmos. Environ., 37, 545–562, doi:10.1016/S1352-2310(02)00886-5, 2003.

Hu, M., He, L. Y., Zhang, Y. H., Wang, M., Kim, Y. P., and Moon, K. C.: Seasonal variation of ionic species in fine particles at Qingdao, China, Atmos. Environ., 36, 5853–5859, doi:10.1016/S1352-2310(02)00581-2, 2002a.

Hu, M., Zhou, F., Shao, K., Zhang, Y., Tang, X., and Slanina, J.: Diurnal variations of aerosol chemical compositions and related gaseous pollutants in Beijing and Guangzhou, J. Environ. Sci. Heal. A, 37, 479–488, doi:10.1081/ese-120003229, 2002b.

Huang, R. J., Zhang, Y., Bozzetti, C., Ho, K. F., Cao, J. J., Han, Y., Daellenbach, K. R., Slowik, J. G., Platt, S. M., Canonaco, F., Zotter, P., Wolf, R., Pieber, S. M., Bruns, E. A., Crippa, M., Ciarelli, G., Piazzalunga, A., Schwikowski, M., Abbaszade, G., Schnelle-Kreis, J., Zimmermann, R., An, Z., Szidat, S., Baltensperger, U., El Haddad, I., and Prevot, A. S.: High secondary aerosol contribution to particulate pollution during haze events in China, Nature, 514, 218–222, doi:10.1038/nature13774, 2014.

Jansen, R. C., Shi, Y., Chen, J., Hu, Y., Xu, C., Hong, S., Li, J., and Zhang, M.: Using hourly measurements to explore the role of secondary inorganic aerosol in $PM_{2.5}$ during haze and fog in Hangzhou, China, Adv. Atmos. Sci., 31, 1427–1434, doi:10.1007/s00376-014-4042-2, 2014.

Ji, D., Li, L., Wang, Y., Zhang, J., Cheng, M., Sun, Y., Liu, Z., Wang, L., Tang, G., Hu, B., Chao, N., Wen, T., and Miao, H.: The heaviest particulate air-pollution episodes occurred in northern China in January 2013: Insights gained from observation, Atmos. Environ., 92, 546–556, doi:10.1016/j.atmosenv.2014.04.048, 2014.

Khoder, M. I.: Atmospheric conversion of sulfur dioxide to particulate sulfate and nitrogen dioxide to particulate nitrate and gaseous nitric acid in an urban area, Chemosphere, 49, 675–684, doi:10.1016/S0045-6535(02)00391-0, 2002.

Pandis, S. N. and Seinfeld, J. H.: Sensitivity analysis of a chemical mechanism for aqueous-phase atmospheric chemistry, J. Geophys. Res.-Atmos., 94, 1105–1126, doi:10.1029/Jd094id01p01105, 1989.

Pathak, R. K. and Chan, C. K.: Inter-particle and gas-particle interactions in sampling artifacts of $PM_{2.5}$ in filter-based samplers, Atmos. Environ., 39, 1597–1607, doi:10.1016/j.atmosenv.2004.10.018, 2005.

ACPD
15, 33407–33443, 2015

Pathak, R. K., Yao, X. H., and Chan, C. K.: Sampling artifacts of acidity and ionic species in $PM_{2.5}$, Environ. Sci. Technol., 38, 254–259, doi:10.1021/Es0342244, 2004.
Pathak, R. K., Wu, W. S., and Wang, T.: Summertime $PM_{2.5}$ ionic species in four major cities of China: nitrate formation in an ammonia-deficient atmosphere, Atmos. Chem. Phys., 9, 1711–1722, doi:10.5194/acp-9-1711-2009, 2009.
Pitchford, M., Maim, W., Schichtel, B., Kumar, N., Lowenthal, D., and Hand, J.: Revised algorithm for estimating light extinction from IMPROVE particle speciation data, J. Air Waste Manage., 57, 1326–1336, doi:10.3155/1047-3289.57.11.1326, 2007.
Polissar, A. V., Hopke, P. K., Paatero, P., Kaufmann, Y. J., Hall, D. K., Bodhaine, B. A., Dutton, E. G., and Harris, J. M.: The aerosol at Barrow, Alaska: long-term trends and source locations, Atmos. Environ., 33, 2441–2458, doi:10.1016/S1352-2310(98)00423-3, 1999.
Quan, J., Tie, X., Zhang, Q., Liu, Q., Li, X., Gao, Y., and Zhao, D.: Characteristics of heavy aerosol pollution during the 2012–2013 winter in Beijing, China, Atmos. Environ., 88, 83–89, doi:10.1016/j.atmosenv.2014.01.058, 2014.
Ramanathan, V. and Vogelmann, A. M.: Greenhouse effect, atmospheric solar absorption and the Earth's radiation budget: from the Arrhenius-Langley era to the 1990s, Ambio, 26, 38–46, 1997.
Tan, J., Duan, J., He, K., Ma, Y., Duan, F., Chen, Y., and Fu, J.: Chemical characteristics of $PM_{2.5}$ during a typical haze episode in Guangzhou, J. Environ. Sci., 21, 774–781, doi:10.1016/s1001-0742(08)62340-2, 2009.
Tao, J., Zhang, L. M., Ho, K. F., Zhang, R. J., Lin, Z. J., Zhang, Z. S., Lin, M., Cao, J. J., Liu, S. X., and Wang, G. H.: Impact of $PM_{2.5}$ chemical compositions on aerosol light scattering in Guangzhou - the largest megacity in South China, Atmos. Res., 135, 48–58, doi:10.1016/j.atmosres.2013.08.015, 2014.
Tao, J., Zhang, L., Gao, J., Wang, H., Chai, F., and Wang, S.: Aerosol chemical composition and light scattering during a winter season in Beijing, Atmos. Environ., 110, 36–44, doi:10.1016/j.atmosenv.2015.03.037, 2015.
Tegen, I., Koch, D., Lacis, A. A., and Sato, M.: Trends in tropospheric aerosol loads and corresponding impact on direct radiative forcing between 1950 and 1990: A model study, J. Geophys. Res.-Atmos., 105, 26971–26989, doi:10.1029/2000jd900280, 2000.
Tie, X., Madronich, S., Li, G., Ying, Z., Weinheimer, A., Apel, E., and Campos, T.: Simulation of Mexico City plumes during the MIRAGE-Mex field campaign using the WRF-Chem model, Atmos. Chem. Phys., 9, 4621–4638, doi:10.5194/acp-9-4621-2009, 2009a.

ACPD
15, 33407–33443, 2015

Tie, X., Wu, D., and Brasseur, G.: Lung cancer mortality and exposure to atmospheric aerosol particles in Guangzhou, China, Atmos. Environ., 43, 2375–2377, doi:10.1016/j.atmosenv.2009.01.036, 2009b.

Wang, H., An, J., Shen, L., Zhu, B., Pan, C., Liu, Z., Liu, X., Duan, Q., Liu, X., and Wang, Y.: Mechanism for the formation and microphysical characteristics of submicron aerosol during heavy haze pollution episode in the Yangtze River Delta, China, Sci. Total Environ., 490, 501–508, doi:10.1016/j.scitotenv.2014.05.009, 2014a.

Wang, H., Xu, J., Zhang, M., Yang, Y., Shen, X., Wang, Y., Chen, D., and Guo, J.: A study of the meteorological causes of a prolonged and severe haze episode in January 2013 over central-eastern China, Atmos. Environ., 98, 146–157, doi:10.1016/j.atmosenv.2014.08.053, 2014b.

Wang, J., Wang, S., Jiang, J., Ding, A., Zheng, M., Zhao, B., Wong, D. C., Zhou, W., Zheng, G., Wang, L., Pleim, J. E., and Hao, J.: Impact of aerosol-meteorology interactions on fine particle pollution during China's severe haze episode in January 2013, Environ. Res. Lett., 9, 094002, doi:10.1088/1748-9326/9/9/094002, 2014.

Wang, Y., Zhuang, G. S., Tang, A. H., Yuan, H., Sun, Y. L., Chen, S. A., and Zheng, A. H.: The ion chemistry and the source of $PM_{2.5}$ aerosol in Beijing, Atmos. Environ., 39, 3771–3784, doi:10.1016/j.atmosenv.2005.03.013, 2005.

Wang, Y., Zhuang, G., Sun, Y., and An, Z.: The variation of characteristics and formation mechanisms of aerosols in dust, haze, and clear days in Beijing, Atmos. Environ., 40, 6579–6591, doi:10.1016/j.atmosenv.2006.05.066, 2006.

Wang, Y., Yao, L., Wang, L., Liu, Z., Ji, D., Tang, G., Zhang, J., Sun, Y., Hu, B., and Xin, J.: Mechanism for the formation of the January 2013 heavy haze pollution episode over central and eastern China, Science China – Earth Sciences, 57, 14–25, doi:10.1007/s11430-013-4773-4, 2014.

Wang, Y. H., Liu, Z. R., Zhang, J. K., Hu, B., Ji, D. S., Yu, Y. C., and Wang, Y. S.: Aerosol physicochemical properties and implications for visibility during an intense haze episode during winter in Beijing, Atmos. Chem. Phys., 15, 3205–3215, doi:10.5194/acp-15-3205-2015, 2015.

Wang, Y. Q., Zhang, X. Y., and Draxler, R. R.: TrajStat: GIS-based software that uses various trajectory statistical analysis methods to identify potential sources from long-term air pollution measurement data, Environ. Modell. Softw., 24, 938–939, doi:10.1016/j.envsoft.2009.01.004, 2009.

ACPD
15, 33407–33443, 2015

Warneck, P.: Chemistry of the natural atmosphere, Academic press, New York, USA, 1999.
Xiao, H. Y. and Liu, C. Q.: Chemical characteristics of water-soluble components in TSP over Guiyang, SW China, 2003, Atmos. Environ., 38, 6297–6306, doi:10.1016/j.atmosenv.2004.08.033, 2004.
Yang, F. M., He, K. B., Ma, Y. L., Zhang, Q., Cadle, S. H., Chan, T., and Mulawa, P. A.: Characterization of carbonaceous species of ambient $PM_{2.5}$ in Beijing, China, J. Air Waste Manage., 55, 984–992, doi:10.1080/10473289.2005.10464699, 2005.
Yang, Y., Liu, X., Qu, Y., Wang, J., An, J., Zhang, Y., and Zhang, F.: Formation mechanism of continuous extreme haze episodes in the megacity Beijing, China, in January 2013, Atmos. Res., 155, 192–203, doi:10.1016/j.atmosres.2014.11.023, 2015.
Yao, X. H., Chan, C. K., Fang, M., Cadle, S., Chan, T., Mulawa, P., He, K. B., and Ye, B. M.: The water-soluble ionic composition of $PM_{2.5}$ in Shanghai and Beijing, China, Atmos. Environ., 36, 4223–4234, doi:10.1016/S1352-2310(02)00342-4, 2002.
Yu, H. B., Liu, S. C., and Dickinson, R. E.: Radiative effects of aerosols on the evolution of the atmospheric boundary layer, J. Geophys. Res.-Atmos., 107, AAC 3-1–AAC 3-14, doi:10.1029/2001jd000754, 2002.
Yu, S., Zhang, Q., Yan, R., Wang, S., Li, P., Chen, B., Liu, W., and Zhang, X.: Origin of air pollution during a weekly heavy haze episode in Hangzhou, China, Environ. Chem. Lett., 12, 543–550, doi:10.1007/s10311-014-0483-1, 2014.
Zhang, J., Chen, J., Yang, L., Sui, X., Yao, L., Zheng, L., Wen, L., Xu, C., and Wang, W.: Indoor $PM_{2.5}$ and its chemical composition during a heavy haze-fog episode at Jinan, China, Atmos. Environ., 99, 641–649, doi:10.1016/j.atmosenv.2014.10.026, 2014.
Zhang, Q., Quan, J., Tie, X., Li, X., Liu, Q., Gao, Y., and Zhao, D.: Effects of meteorology and secondary particle formation on visibility during heavy haze events in Beijing, China, Sci. Total Environ., 502, 578–584, doi:10.1016/j.scitotenv.2014.09.079, 2015.
Zhang, X. Y., Wang, Y. Q., Niu, T., Zhang, X. C., Gong, S. L., Zhang, Y. M., and Sun, J. Y.: Atmospheric aerosol compositions in China: spatial/temporal variability, chemical signature, regional haze distribution and comparisons with global aerosols, Atmos. Chem. Phys., 12, 779–799, doi:10.5194/acp-12-779-2012, 2012.
Zheng, G. J., Duan, F. K., Su, H., Ma, Y. L., Cheng, Y., Zheng, B., Zhang, Q., Huang, T., Kimoto, T., Chang, D., Pöschl, U., Cheng, Y. F., and He, K. B.: Exploring the severe winter haze in Beijing: the impact of synoptic weather, regional transport and heterogeneous reactions, Atmos. Chem. Phys., 15, 2969–2983, doi:10.5194/acp-15-2969-2015, 2015.

ACPD
15, 33407–33443, 2015

Table 1. The percentages of each trajectory cluster and the mean b_{ext} ($M\,m^{-1}$) and mean concentrations ($\mu g\,m^{-3}$) of $PM_{2.5}$ and selected aerosol species in the identified trajectory clusters.

	1	2	3	4	5	6
Percent (%)	20.6	31.7	20.6	12.7	6.3	7.9
$PM_{2.5}$	129	117	167	103	84.0	87.4
OC	21.1	22.8	25.3	16.4	30.5	20.3
EC	2.05	3.87	2.21	1.45	3.90	1.86
Sulfate	22.9	18.2	32.4	23.1	8.85	8.39
Nitrate	11.5	10.0	16.9	7.84	3.26	7.91
Ammonium	15.2	12.3	18.9	12.4	7.93	9.88
b_{ext}	675	597	921	556	548	463

ACPD
15, 33407–33443, 2015

Figure 1. The sampling site in Suzhou. The locations of some major cities with a population of more than 1 million (such as Qingdao, Nanjing and Hangzhou) are marked with a square symbol. The topographical map was derived from Microsoft ® Encarta ® 2009 © 1993–2008.

ACPD
15, 33407–33443, 2015

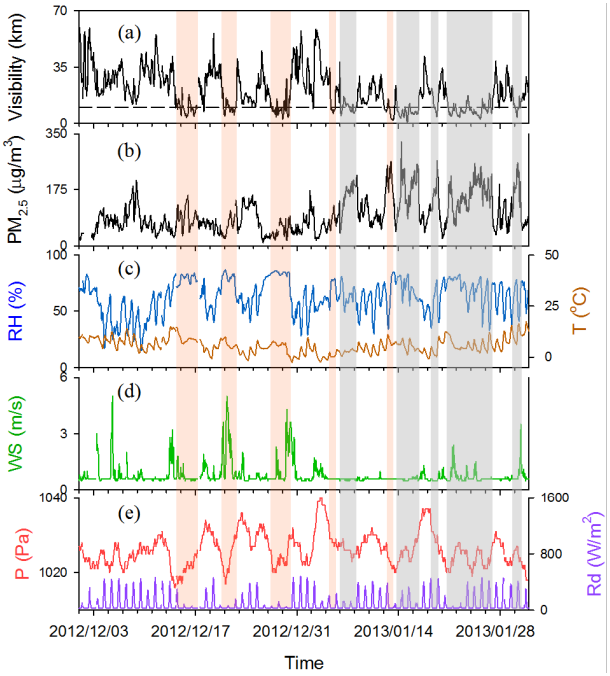

Figure 2. Time series of **(a)** visibility; **(b)** $PM_{2.5}$ concentration; **(c)** relative humidity (RH) and temperature (T); **(d)** wind speed (WS) and pressure (P); **(e)** solar radiation (Rd).

ACPD
15, 33407–33443, 2015

Characteristics of aerosol pollution during heavy haze events

M. Tian et al.

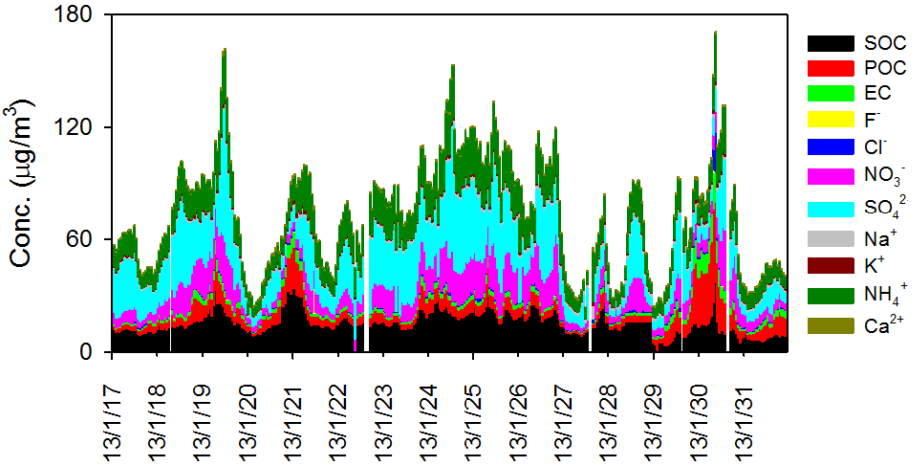

Figure 3. Temporal distribution of water soluble inorganic ions and carbonaceous species.

ACPD
15, 33407–33443, 2015

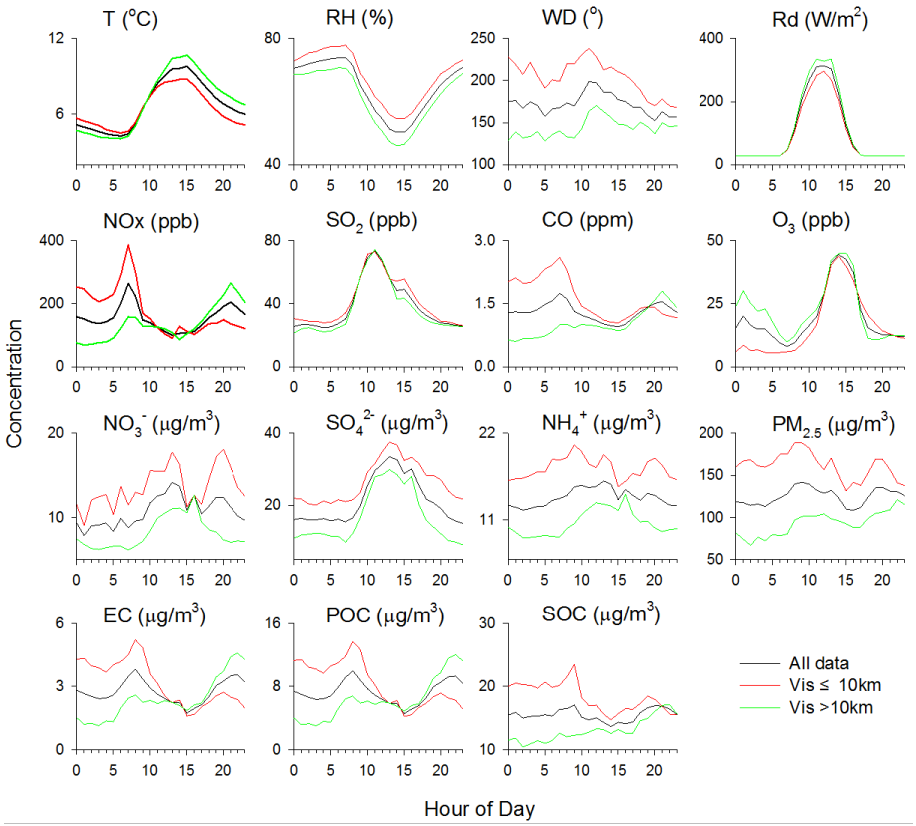

Figure 4. Diurnal profiles of meteorological variables, aerosol precursors (NO_x, SO_2, CO, O_3), $PM_{2.5}$, and major aerosol compounds (NO_3^-, SO_4^{2-}, NH_4^+, EC, POC, SOC) under different visibility conditions.

ACPD
15, 33407–33443, 2015

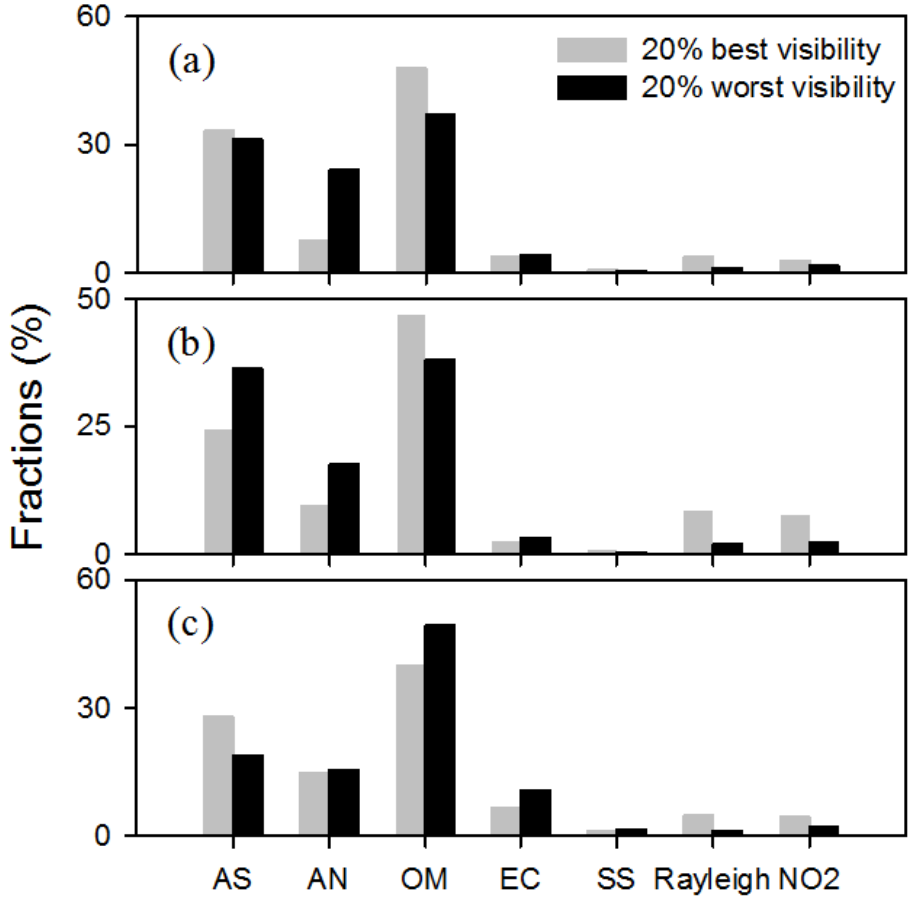

Figure 5. Relative contribution of various chemical components in $PM_{2.5}$ (ammonium sulfate (AS), ammonium nitrate (AN), OM, and EC) to the total light extinction under 20 % best and 20 % worst visibility conditions during the first **(a)**, second **(b)**, and third **(c)** haze events.

ACPD
15, 33407–33443, 2015

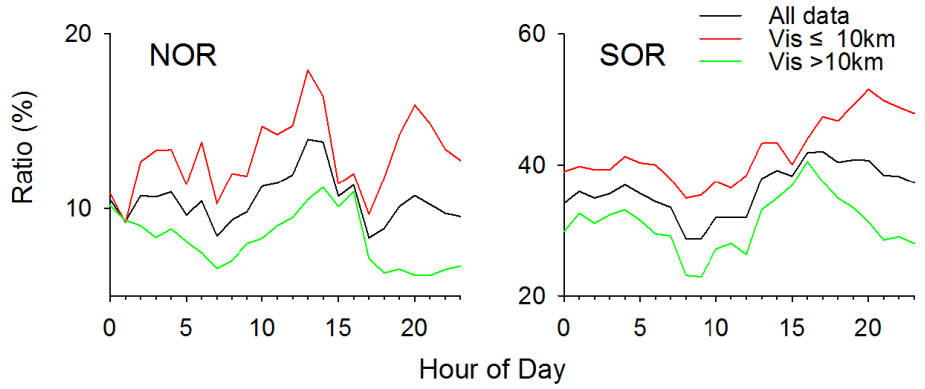

Figure 6. Diurnal profiles of NOR and SOR under different visibility conditions.

ACPD
15, 33407–33443, 2015

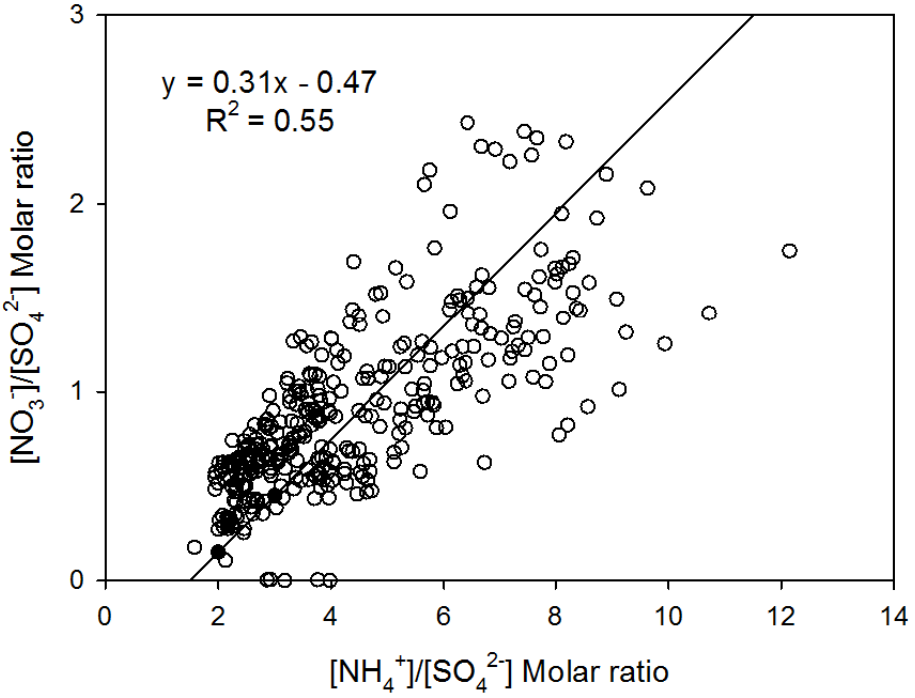

Figure 7. Nitrate to sulfate molar ratio as a function of ammonium to sulfate molar ratio.

ACPD
15, 33407–33443, 2015

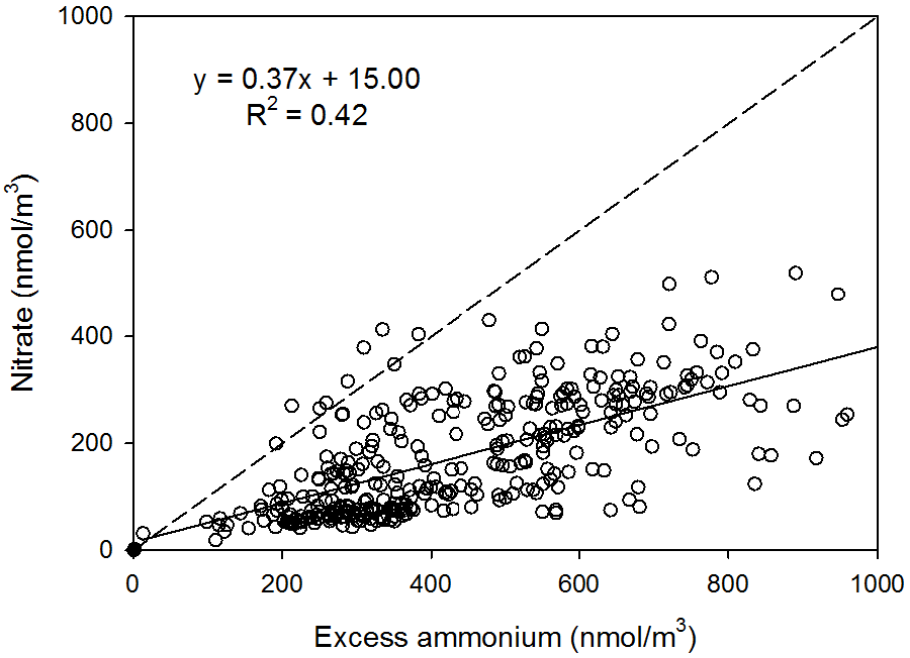

Figure 8. Relationship between molar concentrations of nitrate and excess ammonium.

ACPD
15, 33407–33443, 2015

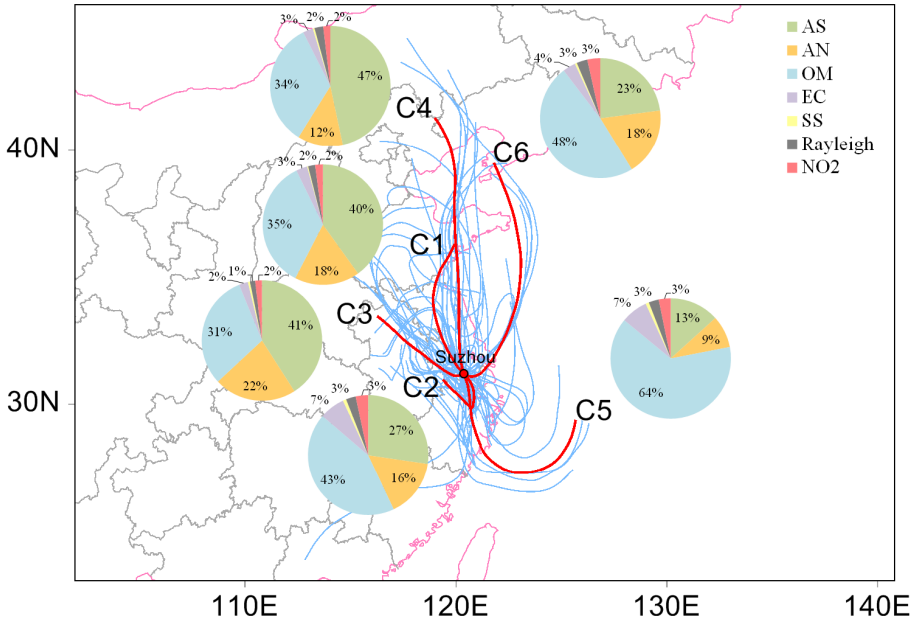

Figure 9. Backward air mass trajectories and six mean trajectories after the cluster analysis at the sampling site during 17 to 31 January. Relative contributions of various chemical components to the total light extinction in different clusters are illustrated.

ACPD
15, 33407–33443, 2015

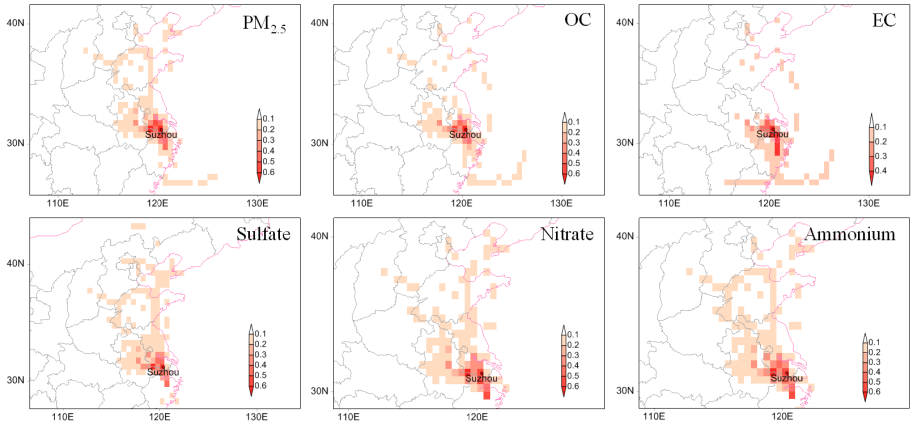

Figure 10. The PSCF maps for $PM_{2.5}$, OC, EC, sulfate, nitrate, and ammonium.

ACPD
15, 33407–33443, 2015

Characteristics of aerosol pollution during heavy haze events

M. Tian et al.